Fan cells in layer 2 of lateral entorhinal cortex are critical for episodic-like memory

Brianna Vandrey[1, 2], Derek L. F. Garden[1], Veronika Ambrozova[2], Christina McClure[1], Matthew F. Nolan[1]*, James A. Ainge[2]*

[1] Centre for Discovery Brain Sciences, University of Edinburgh

[2] School of Psychology & Neuroscience, University of St Andrews

* Equal contributing corresponding authors.

* For correspondence: matt.nolan@ed.ac.uk, jaa7@st-andrews.ac.uk

Abstract

The lateral entorhinal cortex (LEC) is a critical structure for episodic memory, but the roles of discrete neuronal populations within LEC are unclear. Here, we establish an approach for selectively targeting fan cells in layer 2 (L2) of LEC. Whereas complete lesions of the LEC were previously found to abolish associative recognition memory, we find that after selective suppression of synaptic output from fan cells mice still recognise novel object-context configurations, but are impaired in recognition of novel object-place-context associations. Our experiments suggest a segregation of memory functions within LEC networks and indicate that specific inactivation of fan cells leads to behavioural deficits reminiscent of early stages of Alzheimer's disease.

Introduction

Episodic memory relies on the hippocampus and its surrounding cortical network. Within this network, the lateral entorhinal cortex (LEC) and hippocampus are required for episodic-like memory in rodents (Langston & Wood, 2010; Wilson et al. 2013a), and the LEC is critical for integrating spatial and contextual information about objects (Van Cauter et al. 2013; Wilson et al. 2013a; 2013b; Kuruvilla & Ainge, 2017). LEC neurons encode objects within an environment, spatial locations where objects were previously experienced, and generate representations of time during the encoding and retrieval of episodes (Deshmukh & Knierim, 2011; Montchal et al. 2018; Tsao et al. 2013; 2018; Wang et al. 2018). However, it remains unclear how specific populations of cells within the LEC contribute to the integration of episodic memory components.

Projections to the hippocampus from layer 2 (L2) of LEC are of particular interest given that this layer manifests early pathology in Alzheimer's Disease (AD) and related animal models (Gomez-Isla et al. 1996; Stranahan & Mattson, 2010; Khan et al. 2014). These projections arise from a superficial sublayer (L2a) which contains fan cells that are immunoreactive for reelin and project to the dentate gyrus (Fujimara & Kosaka, 1996; Leitner et al. 2016). These neurons appear to have distinct roles in odor information processing by the LEC **(**Leitner et al. 2016). An impaired ability to associate different features in memory is characteristic of early AD (Fowler et al. 2002; O'Connell et al. 2004; Parra et al. 2009; 2010) and although correlations between these deficits and pathology of the superficial entorhinal cortex

suggest contributions to episodic memory processes (Kobro-Flatmoen et al. 2016), the roles of specific cell types in associative memory are unclear.

Here, we ask if suppressing synaptic output from fan cells replicates the behavioural deficits found following complete lesions of the LEC. We show that Sim1:Cre mice, which were previously used to target reelin positive stellate cells in L2 of the medial entorhinal cortex (MEC; Sürmeli et al. 2015, Tennant et al. 2018**)**, can be repurposed to give genetic access to reelin positive fan cells in L2 of LEC. By selectively blocking their synaptic output, we show that fan cells are critical for memory of object-place-context context associations, but are not required for novel object or object-context recognition.

Results

Sim1:Cre mice give genetic access to fan cells in L2 of LEC

Because the arrangement of neurons in L2 of the LEC is similar to L2 of the MEC (Supplemental Figure 1.1; Fujimara & Kosaka et al. 1996; Leitner et al. 2016), we investigated whether Sim1:Cre mice provide specific access to reelin positive fan cells in L2 of the LEC. We found that following injection of Cre-dependent AAV encoding green fluorescent protein (AAV-FLEX-GFP; Murray et al. 2011) into the superficial LEC of Sim1:Cre mice (n = 4), the majority of cells expressing GFP were located in LEC L2a (Figure 1A-B). Staining with antibodies against reelin and calbindin revealed that expression of GFP was specific to cells that were positive for reelin, but not calbindin (Figure 1C-D). A small number of cells were triple-labelled by reelin, calbindin, and GFP (Supplemental Figure 1.2). To establish whether the

labelled population of neurons overlapped with the population of cells that project to the hippocampus, we injected a further cohort of Sim1:Cre mice (n = 3) with AAV-FLEX-GFP into superficial LEC and a retrograde tracer into the dorsal dentate gyrus. The majority of neurons expressing GFP co-localised with neurons labelled by the retrograde tracer (Figure 1E-F). Therefore, the Sim1:Cre mouse provides genetic access to a population of neurons in LEC L2 which are positive for reelin and project to the hippocampus.

L2 of LEC contains several morphologically and electrophysiologically distinct subtypes of neuron, including pyramidal, multi-form, and fan cells (Tahlvidari & Alonso, 2005; Canto & Witter, 2012; Leitner et al. 2016). To establish whether the population of cells labelled in Sim1:Cre mice mapped onto a specific subtype, we injected AAV encoding a Cre-dependent fluorescent reporter (AAV-hSyn-DIO-hM4D(Gi)-mCherry) into the superficial LEC of Sim1:Cre mice (n = 5) and performed patch-clamp recordings in brain slices from labelled cells in L2a of LEC (n = 15 cells). The electrophysiological properties of the labelled cells were consistent with those previously described for fan cells (Figure 2A; Supplemental Table 2.1), including a relatively depolarized resting membrane potential (-68.5 ± 1.4 mV), high input resistance (130.8 ± 11.9 mΩ), slow time constant (24.2 ± 1.7 ms) and a ‘sag’ membrane potential response to injection of hyperpolarizing current (0.85 ± 0.1). Reconstruction of a subset of these cells (n = 12) revealed that their dendritic architecture was similar to previous descriptions of fan cells, with a polygonal soma and ‘fan-like’ arrangement of primary dendrites. To test whether these cells provide synaptic output to the hippocampus, we injected AAV encoding Cre-dependent

79 channelrhodopsin-2 (ChR2; AAV-EF1a-DIO-hChR2(H134R)-EYFP) into the
80 superficial LEC of Sim1:Cre mice (n = 5) to enable their optical activation (Figure
81 2B). We then recorded light-evoked glutamatergic synaptic potentials in downstream
82 granule cells in the dentate gyrus (Figure 2C; n = 6 cells), confirming that the labelled
83 cells mediate perforant path inputs from the LEC to the dentate gyrus.

84 Together, these experiments demonstrate that Sim1:Cre mice can be used to
85 obtain genetic access to fan cells in L2 of the LEC. Our analyses confirm that fan
86 cells express reelin and project to the dentate gyrus of the hippocampus.

87

88 **Fan cells in L2 of LEC are critical for episodic-like memory**

89 To test whether fan cells are required for associative recognition memory, we
90 blocked their output using targeted injections of AAV encoding a Cre-dependent
91 tetanus toxin light chain (TeLC) (Figure 3A; AAV-FLEX-TeLC-GFP), an approach we
92 previously validated for inactivation of stellate cells in L2 of the MEC (Tennant et al.
93 2018). We compared Sim1:Cre mice injected with AAV-FLEX-TeLC-GFP (n = 21)
94 with corresponding control mice injected with AAV-FLEX-GFP (n = 17).

95 We assessed performance of the mice on a series of object-based memory
96 tasks (Figure 3B), which model the integration of episodic memory components in
97 rodents (Eacott & Norman, 2004). In the sample phase of each task, animals
98 encountered two objects in different spatial locations within an environmental context
99 that has distinct visual and tactile features. After a short interval, the animal was
100 presented with a familiar object and an object which was novel or in a novel
101 configuration of location and/or context.

102 Mice expressing TeLC in fan cells were able to distinguish novel objects and
103 object-context configurations. Both TeLC and control mice explored novel objects
104 more than expected by chance, although discrimination ratios were lower for the
105 TeLC group (Figure 3C; $F_{(1,33)}$= 4.542, P= 0.041, η^2 = 0.121). Novel object-context
106 configurations were also explored more than expected by chance by the TeLC and
107 control mice, with no difference between the two groups ($F_{(1,33)}$= 0.275, P = 0.603).
108 These data suggest that fan cells are not required for recognition of novel objects,
109 and unlike the LEC as a whole, are not required for recognition of novel object-
110 context associations.

111 When we investigated discrimination of more complex associations of object,
112 place, and context, we found that mice in the TeLC group showed no exploratory
113 preference for the novel configuration, whereas mice in the control group explored
114 the novel configuration more than predicted by chance. Consistent with this, there
115 was a significant difference in performance between the two groups ($F_{(1,29)}$= 10.319,
116 P = 0.003, η^2 = 0.262). The amount of time spent exploring the objects was similar
117 across groups for all tasks, indicating that differences between groups are not
118 explained by reduced interest in the objects.

119 If deficits in task performance result from expression of TeLC then
120 performance should correlate with the extent to which AAV-FLEX-TeLC-GFP
121 infected fan cells across the LEC. To test this, we quantified for each animal the
122 percentage area of L2 of LEC with virus expression (Figure 4A-B). We found that the
123 pattern of GFP labelling in the older mice used for behavioural experiments was
124 similar to that of younger mice used for electrophysiological and anatomical

experiments (cf. Figures 1A and 4A). When we compared the percentage area of virus expression with object-place-context discrimination we found a negative correlation for the TeLC group (Figure 4C; R = -0.483, n = 18, P = 0.042), but not for the GFP group (R = 0.356, n = 9, P = 0.347). We did not find any correlation between viral expression and performance for the other recognition tasks (Supplemental Figure 4.1).

Discussion

Our data provide evidence that fan cells in L2 of LEC are critical for episodic-like memory. This is in contrast to complete lesions of the LEC, which cause a general associative memory impairment (Wilson et al. 2013a; 2013b). Our data are consistent with a role of the LEC in encoding complex information about objects in the environment (Deshmukh et al. 2011; Tsao et al. 2013; 2018; Wang et al. 2018), and suggest that this information may contribute to the formation of object-place-context associations via projections from fan cells to the hippocampus. Impaired episodic-like memory but spared recognition of simpler associations following lesions of the hippocampus are consistent with this possibility (Langston & Wood, 2010).

Functional specialisation within LEC circuits has implications for normal circuit computations and disorders. Our results suggest a model in which L2a generates outputs specifically required for relatively complex object-place-context associations, whereas neurons in other layers maybe sufficient for formation of simpler associations. Pathology of the superficial LEC has been associated with early cognitive deficits in AD and in age-related cognitive decline (Gomez-Isla et al. 1996;

148 Stranahan et al. 2011a; 2011b; Khan et al. 2014; Kobro-Flatmoen et al. 2016). By
149 showing that episodic-like memory requires output from fan cells, our results suggest
150 that pathology specific to L2a of LEC is sufficient to account for associative memory
151 impairments in early stages of AD.

Materials and Methods

Animals

The Sim1:Cre line, which expresses Cre under the control of the Single minded homolog-1 (Sim1) promoter, was generated by GenSat and obtained from MMRRC (strain name: Tg(Sim1cre)KH21Gsat/Mmucd). Sim1:Cre mice were bred to be heterozygous for the Cre transgene by crossing a male Sim1:Cre mouse carrying the transgene with female C57BL6/J mice. Anatomical and electrophysiological experiments used 5-11 week old mice and the behavioural experiment used 3-8 month old mice. All mice were housed in groups in diurnal light conditions (12-hr light/dark cycle) and had *ad libitum* access to food and water. All experiments and surgery were conducted under project licenses administered by the UK Home Office and in accordance with national (Animal [Scientific Procedures] Act, 1986) and international (European Communities Council Directive of 24 November 1986 (86/609/EEC) legislation governing the maintenance of laboratory animals and their use in scientific research.

Viruses

We used the following adeno-associated viruses: AAV-1/2-FLEX-GFP and AAV-1/2-FLEX-TeLC-GFP (generated in house following protocols described by Murray et al. 2011), AAV2-hSyn-DIO-hM4D(Gi)-mCherry (UNC Vector Core, Chapel Hill, North Carolina, Lot #: AV44362) and AAV2-EF1a-DIO-hChR2(H134R)-EYFP (UNC Vector Core, Chapel Hill, North Carolina, Lot #: AV43780).

175 *Stereotaxic Injection of Tracers and Viruses*

176 Mice were anaesthetised with Isoflurane in an induction chamber before being
177 transferred to a stereotaxic frame. Mice were administered an analgesic
178 subcutaneously, and an incision was made to expose the skull. For retrograde
179 labelling of neurons which project to the hippocampus, Fast Blue (Polysciences,
180 Hirschberg an der Bergstraße, Germany) was injected unilaterally into the dorsal
181 dentate gyrus. A craniotomy was made at 2.8 mm posterior to bregma and 1.8 mm
182 lateral to the midline. A glass pipette was lowered vertically into the brain to a depth
183 1.7 mm from the surface, and 50-100 nl of tracer diluted at 0.5% w/v in dH_2O was
184 injected. For injection of virus into the lateral entorhinal cortex, a craniotomy was
185 made adjacent to the intersection of the lamboid suture and the ridge of the parietal
186 bone, which was approximately 3.8 mm posterior to bregma and 4.0 mm lateral to
187 the midline. From these coordinates, the craniotomy was extended 0.8 mm rostrally.
188 At the original coordinates, a glass pipette was lowered from the surface of the brain
189 at a 10°-12°angle until a slight bend in the pipette indicated contact with the dura.
190 The pipette was retracted 0.2 mm and 150-500 nl of virus was injected. This protocol
191 was repeated at a site 0.2 mm rostral to this site. To target ventral lateral entorhinal
192 cortex, the angle of the pipette was adjusted to 6° - 9° and a third injection was
193 delivered at the rostral injection site. The angle was adjusted within each reported
194 range based on the proximity of the craniotomy to the ridge of the parietal bone. This
195 approach minimised the likelihood of spread of virus into adjacent cortical structures.
196 For all injections, the pipette was slowly retracted after a stationary period of four

197 minutes. Mice were administered an oral analgesic prepared in flavoured jelly after
198 surgery.
199
200 *Immunohistochemistry*
201 For tracer injections, animals were sacrificed 1-2 weeks post-surgery. For anatomical
202 and electrophysiological experiments animals were sacrificed 2-4 weeks post-
203 surgery. Mice were administered a lethal dose of sodium pentobarbital and
204 transcardially perfused with cold phosphate buffered saline (PBS) followed by cold
205 paraformaldehyde (PFA, 4%). Brains were extracted and fixed for a minimum of 24
206 hours in PFA at 4°C, washed with PBS, and transferred to a 30% sucrose solution
207 prepared in PBS for 48 hours at 4°C. Brains were sectioned horizontally at 60 μm on
208 a freezing microtome. For staining against reelin and calbindin, slices were blocked
209 for 2-3 hours in 5% Normal Goat Serum (NGS) prepared in 0.3% PBS-T (Triton).
210 Slices were then transferred to a primary antibody solution prepared in 1% NGS in
211 0.3% PBS-T for 24 hours. Primary antibodies were mouse anti-reelin (MBL, 1:200,
212 Catalogue #: D351-3) and rabbit anti-calbindin D-28K (SWANT, 1:2500, Catalog #:
213 CB-38). Slices were washed with 0.3% PBS-T 3x for 20 minutes before being
214 transferred to a secondary antibody solution prepared in 0.3% PBS-T for 24 hours.
215 Secondary antibodies were AlexaFluor® Goat Anti-Mouse 488 (Catalog #: A-10680
216 and 546 (Catalog #: A-11003) and AlexaFluor® Goat Anti-Rabbit 555 (Catalog #:
217 A27039) and 647 (Catalog #: A27040; Invitrogen, all used at 1:500). Neurotrace
218 640/660 (Catalog #: N21483; Invitrogen, 1:800) was included in the secondary

219 antibody solution as a counterstain. Slices were washed with 0.3% PBS-T 3x for 20
220 minutes and then mounted and cover-slipped with Mowiol.
221
222 *Quantification of Immunohistochemistry*
223 All images were acquired using a Nikon A1 confocal microscope and NIS elements
224 software. For quantification of cells immunolabelled for reelin or calbindin, or labelled
225 by retrograde tracer or fluorescent reporter, 20x z-stacks were acquired of regions of
226 interest (ROI) at 1–2 μm steps. ROIs were regions of L2 of various sizes within the
227 borders of LEC, which were determined by referencing an atlas of the mouse brain
228 (Paxinos & Franklin, 2007). All neurons within each ROI were counted manually.
229 Fractions of labelled cells were determined by calculating for each ROI the number
230 of antibody labelled cells divided by the total number of neurotrace labelled cells.
231 Proportions were averaged across all ROIs from all mice to yield an overall
232 percentage of labelled cells.
233
234 *Slice Electrophysiology*
235 Horizontal brain slices were prepared from 5-11 week old Sim1:Cre mice 2-4 weeks
236 after injection of AAV-hSyn-DIO-hM4D(Gi)-mCherry or AAV-EF1a-DIO-
237 hChR2(H134R)-EYFP into superficial LEC. Mice were sacrificed by cervical
238 dislocation and decapitated. The brains were rapidly removed and submerged in
239 cold cutting artificial cerebrospinal fluid (ACSF) at 4-8°C. The cutting ACSF was
240 comprised of the following (in mM): NaCl 86, NaH_2PO4 1.2, KCl 2.5, $NaHCO_3$25,
241 Glucose 25, Sucrose 50, $CACl_2$ 0.5, $MgCl_2$ 7. The dorsal surface of the brain was

242 glued to a block submerged in cold cutting ACSF and horizontal slices were cut
243 using a vibratome at a thickness of 300-400 μm. Slices were transferred to standard
244 ACSF at 37°C for 15 minutes, then incubated at room temperature for a minimum of
245 45 minutes. Standard ACSF was comprised of the following (in mM): NaCl 124,
246 NaH_2PO4 1.2, KCl 2.5, $NaHCO_3$ 25, Glucose 25, $CaCl_2$ 2, $MgCl_2$ 1. For recordings,
247 slices were transferred to a submerged chamber and maintained in standard ACSF
248 at 35-37°C. Labelled neurons in LEC were identified by their expression of the
249 relevant fluorophore. Neurons were patched in the granule cell layer of the dentate
250 gyrus in regions where there was axonal expression of the virus visible in the outer
251 molecular layer. Whole cell patch-clamp recordings were made using borosilicate
252 electrodes with a resistance of 3-6 MΩ for cells in LEC and 6-10 MΩ for cells in
253 dentate gyrus. Electrodes were filled with an intracellular solution comprised of the
254 following (in mM): K gluconate 130, KCl 10, Hepes 10, $MgCl_2$2, EGTA 0.1, Na_2ATP
255 4, Na_2GTP 0.3, phosphocreatine 10, and 0.5% biocytin (w/v). Recordings were made
256 in current-clamp mode from cells with series resistance ≤ 50 MΩ with appropriate
257 bridge-balance and pipette capacitance neutralisations applied.
258
259 *Recording Protocols*
260 A series of protocols were used to characterise the electrophysiological properties of
261 each cell recorded in LEC or the dentate gyrus, as described previously (Nolan et al.
262 2007; Garden et al. 2008). Sub-threshold membrane properties were measured by
263 examining membrane potential responses to injection of current in hyperpolarizing
264 and depolarizing steps (-160 to 160 pA in 80 pA increments, or -80 to 80 pA in 40 pA

265 increments, each 3 s duration), and to injection of an oscillatory current with a
266 linearly varying frequency (ZAP protocol). Supra-threshold properties were estimated
267 from responses to depolarizing current ramp applied to the cell in a constantly
268 increasing manner to induce action potentials (50 pA/s, 3s). Responses to
269 optogenetic activation of inputs to dentate granule cells were evaluated by
270 stimulation with 470 nm wavelength light for 3 ms at 22.4 mW/mm^2. After recording a
271 baseline response to light stimulation, ionotropic glutamate receptor antagonists for
272 AMPA (NBQX, 10 μM) and NMDA receptors (AP-5, 50 μM) were bath applied, and
273 the response to light stimulation was re-evaluated using the same stimulation
274 protocols. Upon completion of investigatory protocols, diffusion of biocytin into the
275 cell was encouraged by injecting large depolarizing currents into the cell (15 x 4 nA,
276 100 ms steps, 1Hz; Jiang et al. 2015). Each cell was left stationary with the electrode
277 attached for a maximum of one hour before being transferred to PFA (4%) and
278 stored at 4°C for at least 24 hours before histological processing.
279
280 *Analysis of Electrophysiological Data*
281 Electrophysiological data were analysed with AxoGraph (axographx.com), IGOR Pro
282 (Wavemetrics, USA) using Neuromatic (http://www.neuromatic.thinkrandom.com),
283 and customised MATLAB scripts. Input resistance, time constant and time-
284 dependent inward rectification ('sag') were measured from the membrane potential
285 response to injections of hyperpolarizing current (-80 or -40 pA). Input resistance
286 (MΩ) was estimated by dividing the steady-state voltage change from the resting
287 membrane potential by the amplitude of the injected current, time constant (ms) was

288 measured as the time taken for the change in voltage to reach a level 37% above its
289 maximal decrease, and 'sag' was measured as the ratio between the maximum
290 decrease in voltage and the steady-state decrease in voltage. Rheobase (pA) was
291 measured as the minimum amplitude of depolarizing current which elicited an action
292 potential response from the cell. Action potential duration (ms) was measured from
293 the action potential threshold (mV), which was defined as the point at which the first
294 derivative of the membrane potential voltage that exceeded 1 mV/1 ms. Action
295 potential amplitude (mV) was measured as the change in voltage between the action
296 potential threshold and peak. To determine the resonant frequency of the cell,
297 membrane impedance was first calculated by dividing the Fourier transform of the
298 membrane voltage response by the Fourier transform of the input current from the
299 ZAP protocol, which was then converted into magnitude and phase components (see
300 Nolan et al. 2007). The resonant frequency was defined as the input frequency which
301 corresponded to the peak impedance magnitude. To quantify the response of
302 granule cells to optical stimulation, the change in amplitude was measured between
303 the resting membrane potential and peak response during stimulation.
304
305 *Neuron Reconstruction*
306 To reveal the morphology of biocytin filled neurons, fixed slices were washed with
307 PBS 4 times for 10 minutes and transferred to a solution containing AlexaFluor®
308 Streptavidin 488 (Invitrogen, 1:1000 or 1:500, Catalog **#:** S32354) and Neurotrace
309 640/660 (Invitrogen, 1:1000 or 1:500) in 0.3% PBS-T for 24 hours. Slices were
310 washed with PBS-T 4 times for 20 mins and then mounted and cover-slipped with

311 Mowiol. Z-stacks were acquired of filled cells at 1-2 μm steps using a 20x objective
312 on either Nikon A1 or Zeiss LSM800 confocal microscopes. The morphology of cells
313 recorded in LEC were confirmed by visual comparison of the shape of the soma and
314 arrangement of dendrites to published morphological descriptions (Tahvildari &
315 Alonso, 2005; Canto & Witter, 2012; Leitner et al. 2016).
316
317 *Behavioural Apparatus*
318 The test environment was a rectangular wooden box (length 32 cm, width 25.5 cm,
319 height 22 cm) that could be configured to provide two distinct contexts. Context A
320 had black and white vertically striped walls with a smooth white floor. Context B had
321 grey walls with a wire-mesh floor. The environment was lit by two lamps positioned
322 equidistantly from the box. The wall and floor of the environment was cleaned with
323 veterinary disinfectant before each trial. To secure objects in place within the
324 environment, square sections of fastening tape (Dual Lock, 3M) were positioned in
325 each of the upper left and right quadrants of the box floor. Objects were household
326 items of approximately the same size as a mouse and varying in colour, shape, and
327 texture. Objects were matched for similarity in size and complexity when paired for
328 testing. To avoid the use of odour cues, new identical copies of each object were
329 used for each trial, and objects were cleaned with disinfectant after each trial.
330
331 *Design of Behavioural Experiments*
332 Behavioural experiments were carried out in two cohorts of mice. In the main
333 manuscript data from the cohorts are pooled. To control for order and cage effects,

334 each cage contained a mixture of mice from the experimental and control group. The
335 experimenter was blind to the manipulation (delivery of either AAV-FLEX-TeLC-GFP
336 or AAV-FLEX-GFP) during all behavioural experiments and their initial analyses.
337
338 *Habituation*
339 In the week before surgery, the experimenter handled each animal every day for 10
340 minutes in the testing room. Habituation to the test environment commenced one
341 week after surgery and lasted for 5 consecutive days. On day 1, the mice explored
342 each context for 10 minutes with their cage mates. On days 2-5 the mice explored
343 each context for 10 minutes individually. On days 4-5, objects were introduced in the
344 upper left and right quadrants of the test environment. Objects used during
345 habituation were not re-used during testing.
346
347 *Behavioural Tasks*
348 Testing commenced in the week after habituation and occurred in three stages:
349 Novel object recognition (NOR), novel object-context (OC) recognition, and novel
350 object-place-context (OPC) recognition. Novel object-place recognition was also
351 included as a stage in these experiments, but neither experimental group of mice
352 performed above chance level in this task therefore we excluded it from further
353 analysis. Each stage lasted for 4 days. For all sample and test trials, the animal was
354 allowed to explore the environment freely for 3 mins. Between trials, mice were
355 removed to a holding cage for approximately 1 minute while the test environment
356 was configured for the subsequent trial. For each task, the object that was novel at

test, the context, and the quadrants where the novel object or configuration occurred were counterbalanced across animals and experimental conditions. For OC and OPC tasks, the presentation order of context A and B in the sample phase, the context used at test, and the context in which each object was presented during the sample phase were also counterbalanced across animals and conditions. The stages are described here in the order in which they occurred:

1. NOR Task: In the sample trial, mice were presented with two copies of a novel object in one of the contexts (striped or grey walls). In the test trial, mice were presented with a new copy of the object from the sample trial (now familiar) and a novel object in the same context as the sample trial.
2. OC task: In the first sample trial, mice were presented with two copies of a novel object in context A. In a second sample trial, mice were presented with two copies of a different novel object in context B. In the test trial, mice were presented with a single copy of each object within one of the contexts (A or B). At test, both objects are familiar and have been encountered at both locations, but one object has previously been encountered in the test context (familiar OC configuration), whereas the other one has not been encountered in the test context (novel OC configuration).
3. OPC task: In the first sample trial, mice were presented with two different novel objects in context A. In a second sample trial, mice were presented with the same objects in opposite locations in context B. In the test trial, mice were presented with two copies of one of the objects within one of the contexts (A or B). At test, one copy of the object is in a novel location for the test context (novel OPC configuration), whereas the other copy is in a familiar location for the test context (familiar OPC configuration).

382

383 *Histology and Quantification of Virus Expression*

384 Mice were transcardially perfused as described previously. Slices were washed in
385 0.3% PBS-T 3 times for 20 minutes before being transferred to a solution containing
386 Neurotrace 640/660 (Invitrogen, 1:800) prepared in 0.3% PBS-T for 2-3 hours at
387 room temperature. Slices were washed with 0.3% PBS-T 3 times for 20 minutes
388 before being mounted and cover-slipped with Mowiol. Mounted sections were stored
389 at 4°C. All images were acquired using a fluorescent microscope (Zeiss ApoTome)
390 and ZenPro software. To confirm the location and extent of virus expression in each
391 animal, 1:4 sections which contained LEC were imaged at a 10x magnification.
392 Coordinates for each section were determined by referencing an atlas of the mouse
393 brain (Franklin & Paxinos, 2007). Unfolded representations of LEC L2a were
394 generated by adapting procedures previously used to quantify lesions of the
395 entorhinal cortex (Insausti et al. 1997; Steffenach et al. 2005). The anterior and
396 posterior borders of the LEC were determined by the bifurcation of L2, which is
397 absent in adjacent cortical structures. A subset of brains (n = 1 TeLC, 4 GFP)
398 suffered mechanical damage to LEC L2 in > 30% of sections that contained LEC.
399 Removal of these mice from the dataset did not change the interpretation of
400 statistical comparison between groups, therefore they were included in the analysis
401 of behaviour but excluded from analyses which address the relationship between
402 virus expression and behaviour. The length of L2a was measured in ImageJ
403 (https://fiji.sc) using a built-in tool calibrated to the scale of the image. For sections
404 with virus expression, three measurements were extracted: the distance of the

405 region of expression from the anterior LEC border, the length of the region of
406 expression, and the distance of the region of expression from the posterior LEC
407 border. The region of expression was defined as the length of L2a between the most
408 anterior infected neuron and the most posterior infected neuron. These
409 measurements were used to calculate the proportion of LEC L2a in which the virus
410 was expressed for each animal, and averaged across all animals for sections with
411 virus expression across the dorsoventral axis to obtain the mean values used to
412 generate the unfolded representations shown in Figure 4A.

413 Adjacent structures were examined for unintended expression of virus in the
414 TeLC group. There was labelling in LEC L5a in a subset of mice (n = 11). In most
415 cases (n = 8), this was negligible, summating to <10 cells across all sections. In
416 other cases (n = 3), this was approximated to be <5% of the area of LEC L5. Further,
417 there was spread of virus to the region of MEC L2 directly adjacent to LEC in a
418 subset of mice (n = 8), but this was approximated to be <5% of the area of MEC L2
419 in all cases. There was no significant difference between performance of mice with
420 L5 expression or MEC expression and other mice in the TeLC group on any task. To
421 determine the density of virus expression in each slice, each region of expression
422 was imaged at a 20x magnification. For each region, the number of neurons
423 expressing the reporter gene (GFP) and the number of counterstained neurons were
424 quantified manually. From these values, the percentage of infected neurons within
425 each region of expression was calculated as the number GFP of labelled cells
426 divided by the number of Neurotrace labelled cells in the region. These values were

427 averaged across all quantified sections to produce a single density value for each
428 mouse.
429
430 *Analysis of Behavioural Data*
431 All trials were recorded by a camera positioned above the test environment. Footage
432 was scored offline by an experimenter who was blind to experimental condition. To
433 ensure reliability of the scores a random sample of 50% of the trials were rescored
434 by a second experimenter who was also blind to condition. Reliability between
435 scorers was good with an intraclass correlation coefficient of 0.878 (2-way mixed
436 model). For each trial, the amount of time spent exploring each object was
437 measured. Exploration was defined as periods where the animal's nose is within 2
438 cm of the object and oriented towards the object, but the animal was not interacting
439 with the object (eg. biting) or rearing against the object to look out of the test
440 environment. To determine whether the animal had an exploratory preference for the
441 novel object or configuration, a discrimination ratio was calculated for each test trial
442 (Ennaceur & Delacour, 1980). The discrimination ratio is calculated by subtracting
443 the amount of time spent exploring the object in the familiar configuration from the
444 amount of time spent exploring the object in a novel configuration, and then dividing
445 this value by the total exploration time. A positive discrimination ratio indicates an
446 exploratory preference for the object in a novel configuration. For each animal,
447 average discrimination ratios were calculated for each task. A population mean was
448 then calculated for experimental (AAV-FLEX-TeLC-GFP) and control (AAV-FLEX-
449 GFP) groups. Trials where the total exploration time was < 5 seconds during sample

or test were excluded. Where ≥ 3 trials of a task met the criteria for exclusion for an animal, data from that animal was removed from the dataset for that task (NOR, n = 3, 1 TeLC and 2 GFP control; OC, n = 2 GFP control, OPC: n = 7, 2 TeLC and 5 GFP control). Behavioral data are provided in the Supplemental Data document.

Statistical Analysis of Behavioural Data

All statistical analyses were conducted using SPSS (IBM, version 24). To determine whether there was an effect of experimental group, univariate ANOVAs with group (experimental and control) as a between-subjects factor were used for each task. To determine whether the average discrimination ratios for each group were different from chance, one-sample *t*-tests were conducted against a value of 0 for each task. To determine whether there was a relationship between the extent of virus expression and behaviour, Pearson's product-moment correlation coefficients were calculated with percentage area of virus expression as a variable against the average discrimination ratio of each task for each animal. Lines of best fit were calculated for the dataset using the least squares method of linear regression.

Author Contributions

Conceptualization and Methodology, B.V., M.F.N., J.A.A., Investigation, B.V., D.L.F.G., V.A., Resources, C.M., Writing - Original Draft, B.V., Writing, Review & Editing, B.V., M.F.N., J.A., Supervision, M.F.N. and J.A., Funding Acquisition, B.V., M.F.N., J.A.

Funding Acknowledgements

This work was supported by a Carnegie Trust Collaborative Research Grant to J.A. and M.F.N, a Henry Dryerre scholarship from the Royal Society of Edinburgh to B.V., and grants from Wellcome Trust (200855/Z/16/Z) to M.F.N, and BBSRC (BB/M025454/1) to M.F.N.

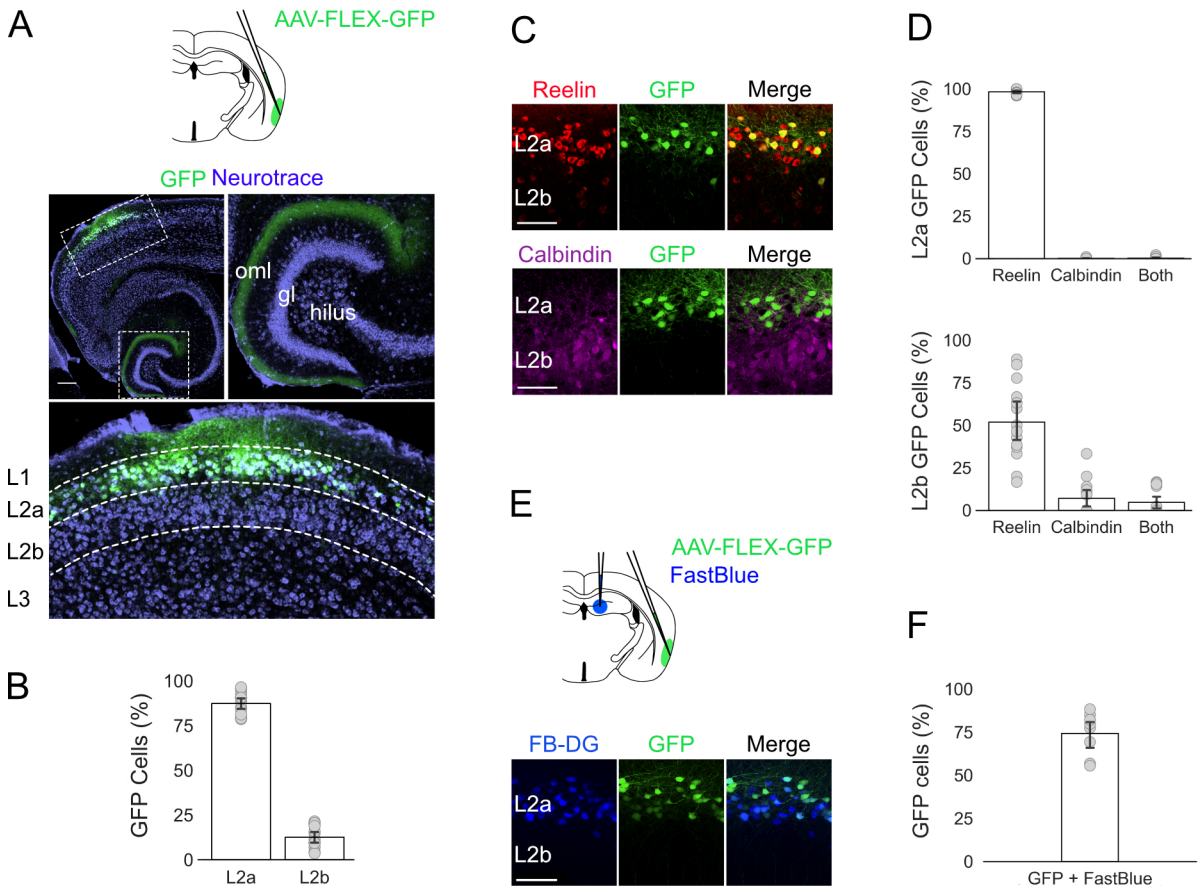

Figure 1: Sim1:Cre mice provide genetic access to reelin cells in L2 of LEC which project to the dentate gyrus. A) Schematic for targeting superficial LEC with AAV-FLEX-GFP and images of a horizontal brain section from a Sim1:Cre mouse showing GFP expression (green) counterstained with Neurotrace (violet). The dashed boxes in the upper left image indicate regions shown in the insets. Axonal labelling is found in the outer molecular layer of the dentate gyrus (upper right) and L2 of LEC (lower). Abbreviations: gl, granule cell layer; oml, outer molecular layer. The scale bar is 250 μm. B) Percentage of neurons that expressed the reporter gene that were in L2a (left, n = 4 mice, 87.4 ± 1.6%, 1282/1490 cells, 14 sections) and L2b (right, 12.6 ± 1.6%, 207/1490 cells) of the LEC. Grey dots indicate percentage values calculated for each section of tissue. Error bars represent SEM. C) Examples of AAV-FLEX-GFP labelled cells which are positive for reelin (red, L2a: 98.3 ± 0.4%, 1260/1282 cells; L2b: 52.0 ± 5.7%, 97/207 cells), but not calbindin (purple, L2a: 0.1 ± 0.1%, 1/1282 cells; L2b: 7.1 ± 2.8%, 17/207 cells). Scale bars represent 100 μm. D) Proportion of neurons expressing the reporter gene (GFP) that were labelled by staining with antibodies against reelin and

494 calbindin. Grey dots indicate percentage values calculated for each section of tissue. Error bars
495 represent SEM. E) Cells labelled by injection of retrograde tracer (blue) overlap with cells labelled by
496 injections of AAV-FLEX-GFP. Scale bar represents 100 μm. Schematic shows the injection strategy
497 used to target superficial LEC with AAV-FLEX-GFP (green) and the dorsal dentate gyrus with a
498 retrograde tracer (Fastblue, blue). F) Proportion of neurons expressing the reporter gene (GFP) that
499 were back-labelled by the injection of retrograde tracer into the dentate gyrus (74.3 ± 4.4%, 331/441
500 cells, 8 sections). Grey dots indicate percentage values calculated for each tissue section. Error bar
501 represents SEM.

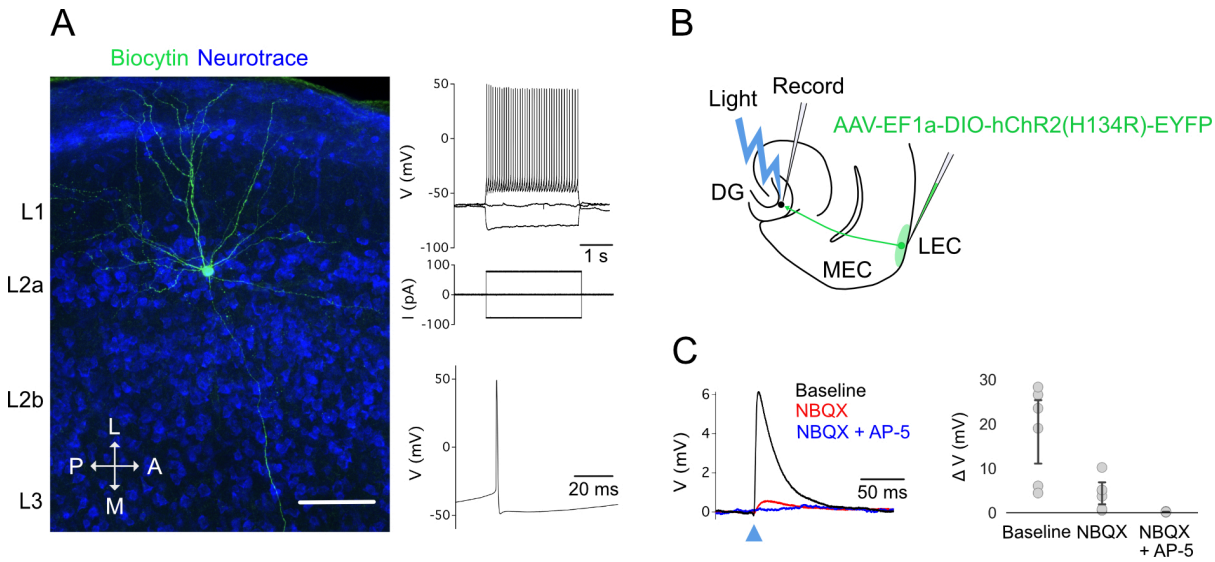

Figure 2: Neurons labelled by Sim1:Cre mice in layer 2 of LEC are fan cells. A) Representative example of the morphology and electrophysiology of a fan cell which expressed mCherry after injection of AAV-hSyn-DIO-hM4D(Gi)-mCherry into the superficial LEC of a Sim1:Cre mouse. (Left) The dendrites and axons of the cell are filled with biocytin (green) and neurons are counterstained with Neurotrace (blue). Note the axon leading towards the dentate gyrus. Scale bar represents 100 µm. (Right) Membrane potential response to the injection of negative and positive current steps (top) and example action potential (bottom). B) Schematic of recording experiment to confirm that fan cells labelled in Sim1:Cre mice project to the dentate gyrus. AAV-EF1a-DIO-ChR2(H134R)-EYFP was injected into the superficial LEC of Sim1:Cre mice (n = 5). Synaptic output from fan cells in layer 2 of LEC was evaluated by recording light evoked responses of granule cells in the dentate gyrus. C) Membrane potential response of a dentate gyrus granule cell after optogenetic activation of fan cells in layer 2 of LEC expressing ChR2. (Left) The peak response was abolished by application of ionotropic glutamate receptor antagonists NBQX (red) and AP-5 (blue). (Right) Quantification of the light evoked membrane potential response of dentate gyrus granule cells (n = 6) after application of NBQX and AP-5. Each grey circle represents an individual neuron. Error bars are SEM.

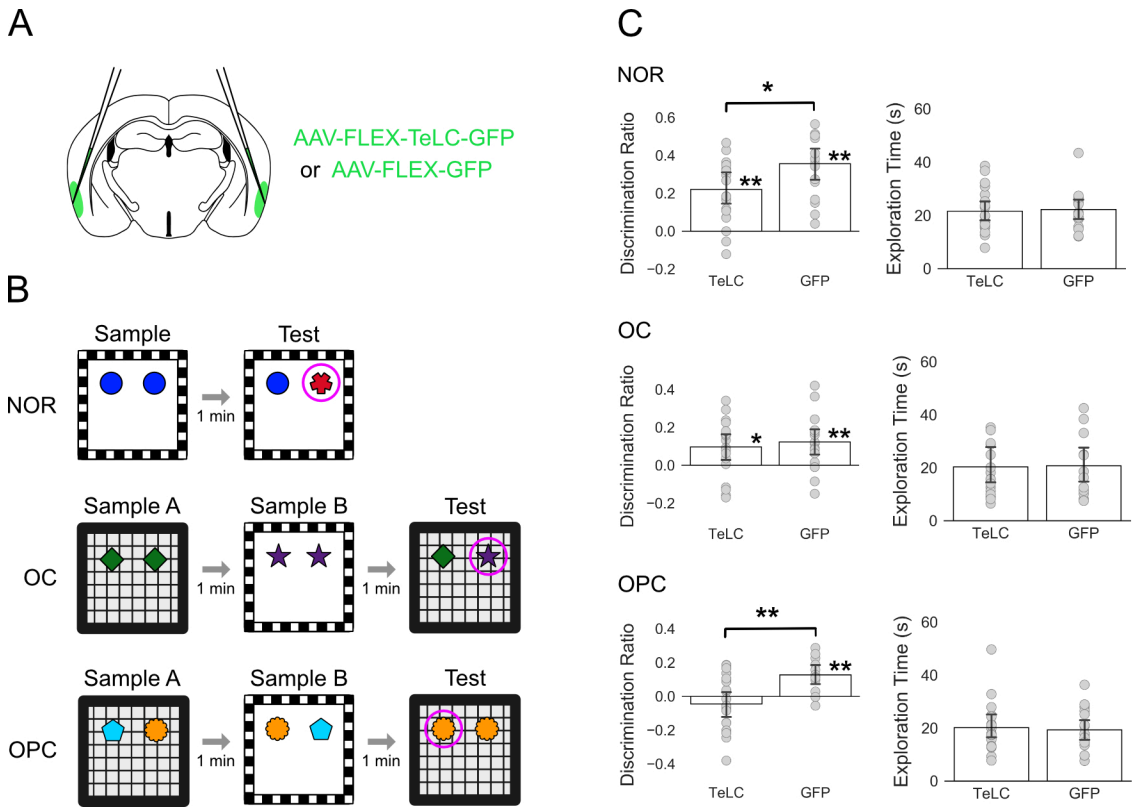

Figure 3: Suppression of fan cells in L2 of LEC impairs performance on the object-place-context task. A) Schematic of injection strategy used to bilaterally target superficial LEC with AAV-FLEX-TeLC-GFP or AAV-FLEX-GFP. B) Schematic of object recognition tasks. Tasks included novel object recognition (NOR, top), object-context (OC, middle) and object-place context (OPC, bottom). Purple circles highlight the novel object or configuration in the test trial. C) Average discrimination ratios (D') and exploration times for each task. Discrimination ratios reflect the proportion of time spent exploring the novel object or configuration (Ennaceur et al. 1980). (Left) Bars indicate average discrimination ratio for each group. One-sample *t*-tests against a value of 0 revealed that mice in both groups performed significantly above chance on the NOR task (top, TeLC: $t(18) = 5.001$, $P < 0.001$; GFP control: $t(15) = 7.922$, $P < 0.001$) and the OC task (middle, TeLC: $t(18) = 2.742$, $P = 0.013$, GFP control: $t(15) = 3.340$, $P = 0.004$). In contrast, mice in the TeLC group showed no exploratory preference for the novel configuration in the OPC task (bottom, $t(18) = -1.183$, $P = 0.252$), whereas mice in the control group explored the novel configuration more than predicted by chance ($t(11) = 4.274$, $P = 0.001$). Univariate ANOVAs revealed a significant difference in performance between TeLC

535 mice and control mice for the NOR (P = 0.041) and OPC tasks (P = 0.003), but not the OC task (P =
536 0.603). Asterisks indicate a significant difference between groups or performance that is significantly
537 different from chance (* = $P < 0.05$, ** = $P < 0.01$). (Right) Bars indicate average exploration time in
538 seconds during the test trials for each group. Each grey dot represents the data for a single animal.
539 Error bars represent SEM.

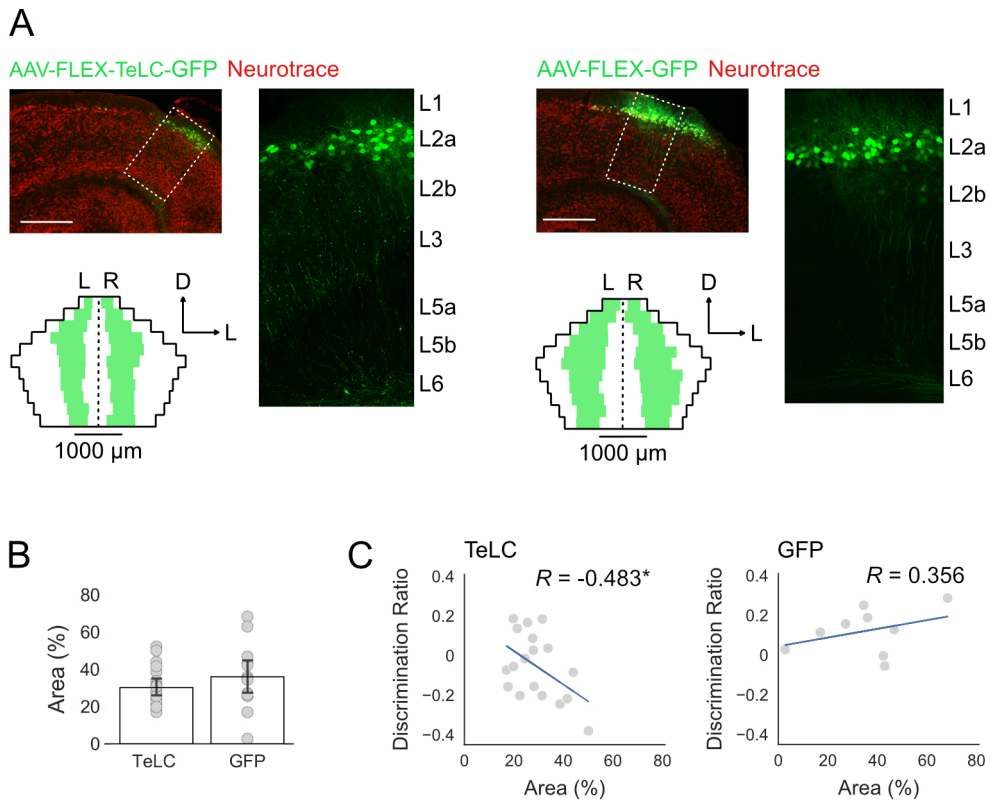

540

541

542 **Figure 4: Quantification of virus expression in mice injected with AAV-FLEX-TeLC-GFP or**
543 **AAV-FLEX-GFP.** A) Horizontal brain sections showing expression of AAV-FLEX-TELC-GFP (left) or
544 AAV-FLEX-GFP (right) in a Sim1:Cre mouse (upper left). Reporter gene expression (GFP, green) is
545 shown against neurons counterstained with Neurotrace (red). Scale bar represents 250 µm. The
546 dashed boxes indicate the regions of LEC which are shown in the insets (right). Unfolded
547 representations of LEC L2a (bottom) are overlaid with the average location and spread of virus
548 expression for each group. Average distances between regions of virus expression and the borders of
549 LEC (white) and average lengths of virus expression (green) were calculated by averaging
550 measurements across all animals for sections at each dorsoventral coordinate of LEC (D = dorsal, L =
551 lateral). Left and right hemispheres are indicated by L and R, and black dotted line indicates
552 separation between hemispheres. B) Bars indicate average percentage area of L2 of LEC which
553 contained neurons that expressed the reporter gene after injection of AAV-FLEX-TELC-GFP or AAV-
554 FLEX-GFP. Each grey dot represents the data for a single animal. Error bars are SEM. C)
555 Relationship between virus expression and performance for the OPC task. Scatterplots of the
556 percentage area of virus expression in LEC L2 plotted against the discrimination ratios for the OPC

557 task. Each grey dot represents data for a single animal. Pearson's correlation coefficients (*R*) were
558 calculated to determine the strength of the relationship between discrimination ratios and virus
559 expression. There was a significant negative correlation between discrimination ratios and virus
560 expression in the TeLC group ($P = 0.042$), but not the GFP group ($P = 0.347$). Asterisks indicate a
561 significant correlation between discrimination ratios and virus expression (* = $P < 0.05$). Each plot is
562 overlaid with the line of best fit (blue) that was calculated using the least squares method of linear
563 regression.

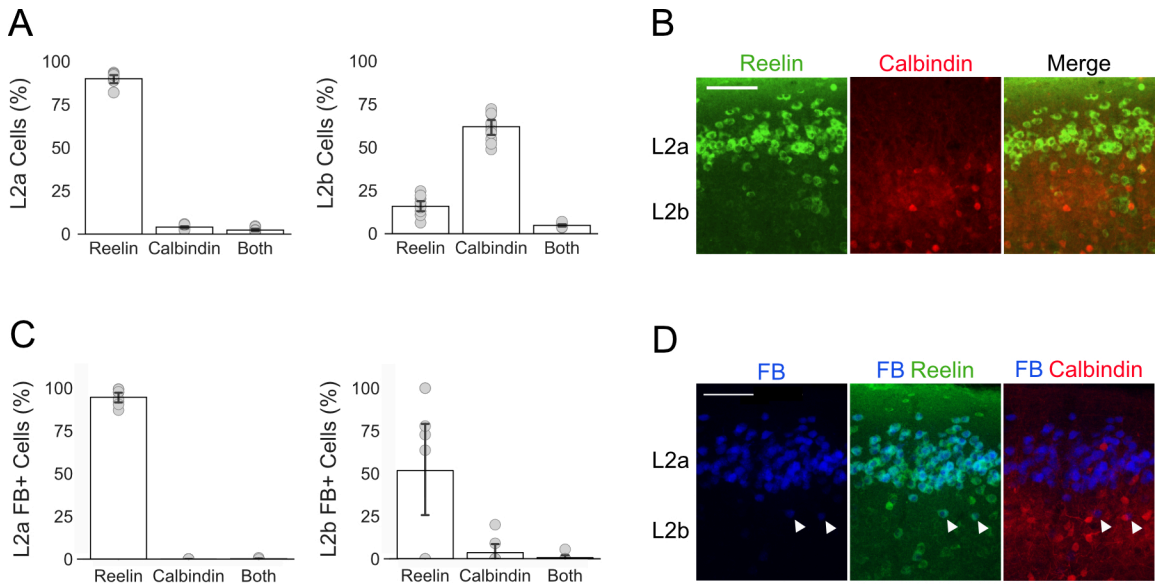

Supplemental Figure 1.1: Quantification of reelin, calbindin and retrograde tracer labelling across sub-layers of LEC L2. A) Quantification of cells positive for reelin and calbindin in LEC L2a (left) and L2b (right; n = 4 mice). Note that the majority of cells in LEC L2a and L2b are positive for reelin and calbindin, respectively, as reported by Leitner et al. (2016). Grey dots indicate percentage values calculated for each section of tissue. Error bars represent SEM. B) Immunolabelling against reelin (green) and calbindin (red) in L2a and L2b of LEC. C) Quantification of cells back-labelled by the retrograde tracer which were positive for reelin and calbindin in LEC L2a (left) and L2b (right; n = 4 mice). Note that the majority of back-labelled cells are positive for reelin in both sub-layers. Grey dots indicate percentage values calculated for each section of tissue. Error bars represent SEM. D) Immunolabelling against reelin (green) and calbindin (red) overlaid with neurons that were back-labelled by the injection of the retrograde tracer FastBlue (FB) into the dentate gyrus (blue). White arrows indicate back-labelled neurons in LEC L2b which are positive for reelin. Scale bars represent 100 µm.

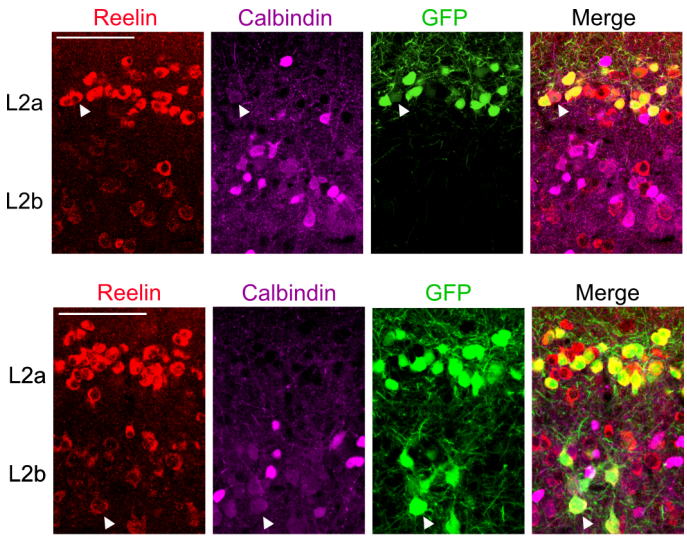

579

580

581 **Supplemental Figure 1.2: Triple-labelling of neurons in L2 of LEC.** Cells triple-labelled by reelin

582 (red), calbindin (purple) and the reporter gene (GFP, green) are indicated by white arrows. A small

583 population of cells was triple-labelled in L2a (top, 0.3 ± 0.2%, 4/1282 cells) and L2b (bottom, 4.6 ±

584 1.9%, 13/207 cells). Scale bars represent 100 μm.

Property	Average	SD	SEM
Resting membrane potential (mV)	-68.47	5.22	1.35
Input resistance (mΩ)	130.47	45.97	11.87
Time constant (ms)	24.19	6.64	1.71
Sag	0.85	0.07	0.02
Rheobase (pA)	126.43	34.36	8.87
Action potential threshold (mV)	-37.95	5.84	1.51
Action potential width (ms)	0.67	0.07	0.02
Action potential amplitude (mV)	88.19	3.65	0.94
Resonance frequency (Hz)	1.15	0.35	0.09
Resonance magnitude (mV)	1.03	0.05	0.01

Supplemental Table 2.1: Electrophysiological properties of fan cells. Table contains the population average, standard deviation (SD) and standard error of the mean (SEM) values for the electrophysiological properties of fan cells (n= 15, 5 mice) in LEC L2 which expressed the reporter gene (mCherry) after injection of AAV-hSyn-DIO-hM4D(Gi)-mCherry into the superficial LEC.

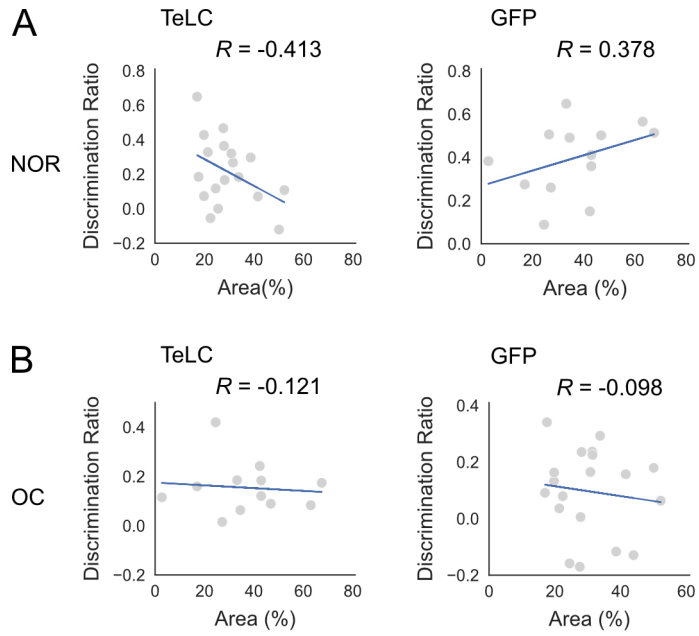

591

592

593 **Supplemental Figure 4.1**: Relationship between virus expression and performance for novel object
594 recognition (NOR) and object-context (OC) tasks. Scatterplots of the percentage area of virus
595 expression in L2 plotted against the discrimination ratios for the NOR (A) and OC task (B). Each grey
596 dot represents data for a single animal. Pearson's correlation coefficients (*R*) were calculated to
597 determine the strength of the relationship between discrimination ratios and virus expression. The
598 exact value of *R* is indicated in the top right corner of each plot. There was no significant correlation
599 between discrimination ratios and virus expression in either group for the NOR (TeLC: $P = 0.089$;
600 GFP control: $P = 0.202$) or OC task (TeLC: $P = 0.622$; GFP control: $P = 0.762$). Each plot is overlaid
601 with line of best fit (blue) that was calculated using the least squares method of linear regression.

602

603 **References**

604 Canto, C. B. & Witter, M. P. (2012). Cellular properties of principal neurons in the rat
605 entorhinal cortex. I. The lateral entorhinal cortex. *Hippocampus*,*22(6)*, 1256-
606 1276.

607 Deshmukh, S.S., & Knierim, J.J. (2011). Representation of non-spatial and spatial
608 information in the lateral entorhinal cortex. *Frontiers in Behavioural*
609 *Neuroscience, doi: 10.3389/fnbeh.2011.00069*.

610 Eacott, M. J., & Norman, G. (2004). Integrated memory for object, place and context
611 in rats: a possible mode of episodic-like memory? *Journal of*
612 *Neuroscience,*24(8), 1948-1953.

613 Ennaceur, A., & Delacour, J. (1988). A new one-trial test for neurobiological studies
614 of memory in rats. 1: Behavioral data. *Behavioural Brain Research, 31(1)*, 47-
615 59.

616 Fowler, K. S., Saling, M. M., Conway, E. L., Semple, J. M., & Louis, W. J. (2002).
617 Paired associate performance in the early detection of DAT. *Journal of the*
618 *International Neuropsychological Society, 8,* 58-71.

619 Fujimaru, Y. & Kosaka, T. (1996). The distribution of two calcium binding proteins,
620 calbindin D-28K and parvalbumin, in the entorhinal cortex of the adult mouse.
621 *Neuroscience Research, 24(4),* 329-343.

622 Garden, D. L. F., Dodson, P. D., O'Donnel, C., White, M. D., & Nolan, M. F. (2008).
623 Tuning of synaptic integration in the medial entorhinal cortex to the
624 organization of grid cell firing fields. *Neuron, 60(5),* 875-889.

Gomez-Isla, T., Price, J. L., McKeel, D. W., Morris, J. C., Growdon, J. H., & Hyman, B. T. (1996). Profound loss of layer II entorhinal cortex neurons occurs in very mild Alzheimer's disease. *Journal of Neuroscience, 16(14),*4491-4500.

Insausti, R., Herrero, M. T., Witter, M. P. (1997). Entorhinal cortex of the rat: Cytoarchitectonic subdivisions and the origin and distribution of cortical efferents. *Hippocampus, 7(2)*,146-183. doi: 10.1002/(SICI)1098-1063(1997)7:2<146::AID-HIPO4>3.0.CO;2-L.

Khan, U. A., Liu, L., Provenzano, F. A., Berman, D. E., Profaci, C. P., Sloan, R., Mayeux, R., Duff, K. E., Small, S. A. (2014). Molecular drives and cortical spread of lateral entorhinal cortex dysfunction in preclinical Alzheimer's disease. *Nature Neuroscience, 17(2)*, 304-311.

Kobro-Flatmoen, A., Nagelhus, A., Witter, M. P. (2016). Reelin-immunoreactive neurons in entorhinal cortex layer II selectively express intracellular amyloid in early Alzheimer's Disease. *Neurobiology of Disease, 93,* 172-183.

Kuruvilla, M. V. & Ainge, J. A. Lateral entorhinal cortex lesions impair local spatial frameworks. *Frontiers in Systems Neuroscience, 11(30),* doi: 10.3389/fnsys.2017.00030.

Leitner, F. C., Melzer, S., Lutcke, H., Pinna, R., Seeburg, P. H., Helmchen, F., & Monyer, H. (2016). Spatially segregated feedforward and feedback neurons support differential odor processing in the lateral entorhinal cortex. *Nature Neuroscience.* doi:10.1038/nn.4303.

Nolan, M. F., Dudman, J. T., Dodson, P. D., & Santoro, B. (2007). HCN1 channels control resting and active integrative properties of stellate cells from layer II of

the entorhinal cortex. *The Journal of Neuroscience, 27(46)*, 12440-12451.

Nature Neuroscience,

Montchal, M. E., Reagh, Z. M., & Yassa, M. A. (2019). Precise temporal memories are supported by the lateral entorhinal cortex in humans. doi: 10.1038/s41593-018-0303-1.

Murray, A. J., Sauer, J-F., Riedel, G., McClure, C., Ansel, L., Cheyne, L., Bartos, M., Wisden, W., & Wulff, P. (2011) Parvalbumin-positive CA1 interneurons are required for spatial working but not for reference memory. *Nature Neuroscience, 14,* 297-299. doi:10.1038/nn.2751.

O'Connell, H., Coen, R., Kidd, N., Warsi, M., Chin, A-V., & Lawlor, B. A. (2004). Early detection of Alzheimer's disease (AD) using the CANTAB paired associates learning test. *International Journal of Geriatric Psychiatry, 19,* 1207-1208.

Parra, M. A., Abrahams, S., Fabi, K., Logie, R., Luzzi, S., Della Sala, S. (2009). Short-term memory binding deficits in Alzheimer's disease. *Brain*, *132,* 1057-1066.

Parra, M. A., Abrahams, S., Logie, R. H., Mendez, L. G., Lopera, F., & Della Sala, S. (2010). Visual short-term memory binding deficits in familial Alzheimer's disease. *Brain, 133,* 2702-2713.

Steffenach, H-A., Witter, M., Moser, M-B., & Moser, E-I. (2005). Spatial memory in the rat required the dorsolateral band of the entorhinal cortex. *Neuron, 45(7)*, 301-313.

670 Stranahan, A. M., Haberman, R.P., & Gallagaher, M.(2011a). Cognitive decline is
671 associated with reduced reelin expression in the entorhinal cortex of aged
672 rats. *Cerebral Cortex, 21(2)*, 392- 400. doi: 10.1093/cercor/bhq106.
673 Stranahan, A. M., Mattson, M. P. (2010). Selective vulnerability of neurons in layer II
674 of the entorhinal cortex during aging and Alzheimer's disease. *Neural*
675 *Plasticity,* doi:10.1155/2010/108190.
676 Stranahan, A. M., Salas-Vaga, S., Jiam, N. T., & Gallagher, M. (2011b). Interference
677 with reelin signalling in the lateral entorhinal cortex impairs spatial memory.
678 *Neurobiology of Learning & Memory, 96(2),*150-155. doi:
679 10.1016/j.nlm.2011.03.009.
680 Sürmeli, G., Marcu, D. C., McClure, C., Garden, D. L. F., Pastoll, H., & Nolan, M. F.
681 Molecularly defined circuitry reveals input-output segregation in deep layers of
682 the medial entorhinal cortex. *Neuron, 88(5),*1040-1053.
683 Tahvildari, B., & Alonso, A. (2005). Morphological and electrophysiological properties
684 of lateral entorhinal cortex layers II and III principal neurons. *Journal of*
685 *Comparative Neurology, 491(2),* 123-140.
686 Tennant, S. A., Fischer, L., Garden, D. L. F., Gerlei, K. Z., Martinez-Gonzalez, C.,
687 McClure, C., Wood, E., & Nolan, M. F. (2018). Stellate cells in the medial
688 entorhinal cortex are required for spatial learning. *Cell Reports, 22(5),* 1313-
689 1324.
690 Tsao, A. Moser, M. B., Moser E. I. (2013). Traces of experience in the lateral
691 entorhinal cortex. *Current Biology, 23(5)*, 399-405.

Tsao, A., Sugar, J., Lu, L., Wang, C., Knierim, J. J., Moser, M-B., Moser, E. I. (2018). Integrating time from experience in the lateral entorhinal cortex. *Nature, 561,* 57-62.

Van Cauter, T., Camon, J., Averabe, A., Eduayen, C., Sargolini, F., & Save, Etienne. (2012). Distinct roles of medial and lateral entorhinal cortex in spatial cognition. *Cerebral Cortex, 23,* 451-459. doi: 10.1093/cercor/bhs033.

Wang, C., Chen, X., Lee, H., Deshmukh, S. S., Yoganarasimha, D., Savelli, F., & Knierim, J. J. (2018). Egocentric coding of external items in the lateral entorhinal cortex. *Science, 362,* 945-949.

Wilson, D. I. G., Langston, R. F., Schlesiger, M. I., Wagner, M., Watanabe, S. & Ainge, J. A. (2013a). Lateral entorhinal cortex is critical for novel object-context recognition. *Hippocampus, 23(5),* 352-366.

Wilson, D. I. G, Watanabe, S., Milner, H., & Ainge, J. A. (2013b). Lateral entorhinal cortex is necessary for associative but not nonassociative recognition memory. *Hippocampus, 23(12),*1280-1290.

Yoo, S. & Lee, I. (2017). Functional double dissociation within the entorhinal cortex for visual scene-dependent choice behaviour. *eLife,* doi: 107554/eLife.21543.001.